PET Imaging of Peripheral Benzodiazepine Receptor Standard Uptake Value Increases After Controlled Cortical Impact, a Rodent Model of Traumatic Brain Injury

Benjamin M. Aertker[1], Akshita Kumar[1], Fanni Cardenas[1] (ORCID),
Franciska Gudenkauf[1] (ORCID), David Sequeira[1], Alan R. Prossin[2],
Amit K. Srivastava[1], Charles S. Cox Jr[1], and Supinder S. Bedi[1] (ORCID)

Abstract

Traumatic brain injury (TBI) is a chronic, life threatening injury for which few effective interventions are available. Evidence in animal models suggests un-checked immune activation may contribute to the pathophysiology. Changes in regional density of active brain microglia can be quantified in vivo with positron emission topography (PET) with the relatively selective radio-tracer, peripheral benzodiazepine receptor 28 (11 C-PBR28). Phenotypic assessment (activated vs resting) can subsequently be assessed (ex vivo) using morphological techniques. To elucidate the mechanistic contribution of immune cells in due to TBI, we employed a hybrid approach involving both in vivo (11 C-PBR28 PET) and ex vivo (morphology) to elucidate the role of immune cells in a controlled cortical impact (CCI), a rodent model for TBI. Density of activated brain microglia/macrophages was quantified 120 hours after injury using the standardized uptake value (SUV) approach. Ex vivo morphological analysis from specific brain regions using IBA-1 antibodies differentiated ramified (resting) from amoeboid (activated) immune cells. Additional immunostaining of PBRs facilitated co-localization of PBRs with IBA-1 staining to further validate PET data. Injured animals displayed greater PBR28suv when compared to sham animals. Immunohistochemistry demonstrated elevated density of amoeboid microglia/macrophages in the ipsilateral dentate gyrus, corpus callosum, thalami and injury penumbra of injured animals compared to sham animals. PBR co-stained with amoeboid microglia/macrophages in the injury penumbra and not with astrocytes. These data suggest the technologies evaluated may serve as bio-signatures of neuroinflammation following severe brain injury in small animals, potentially enabling in vivo tracking of neuroinflammation following TBI and cellular-based therapies.

Traumatic Brain Injury (TBI) causes a prolonged secondary neuroinflammatory response within the central nervous system (CNS) that leads to neurological deficits, both motor and cognitive, beyond that caused by the primary injury (Sandhir et al., 2008; Smith, 2010; Ramlackhansingh et al., 2011). Central to the secondary inflammatory response after TBI are the activation of resident microglia, the macrophages of the CNS (Nakajima and Kohsaka, 2001). Microglia promote learning dependent synapse formation, axonal

[1]Department of Pediatric Surgery, University of Texas Medical School at Houston, Texas, United States
[2]Department of Psychiatry and Behavioral Sciences, University of Texas Medical School at Houston, Texas, United States

Corresponding Author:
Supinder S. Bedi, Department of Pediatric Surgery, University of Texas Medical School at Houston, 6431 Fannin Street, MSB 5.230, Houston, TX 77030, United States.
Email: Supinder.Bedi@uth.tmc.edu

regeneration, and removal of defunct axon terminals (Graeber, 2010; Salter and Beggs, 2014). Under homeostasis, microglia are highly mobile and provide continuous surveillance of their cellular milieu (Davalos et al., 2005; Nimmerjahn et al., 2005). These "resting" or ramified microglia possess a distinct morphology – small, relatively stable rod-shaped somata with thin ramified withdrawing processes (Nimmerjahn et al., 2005).

After TBI, due to the disruption of the blood brain barrier (BBB) there is an influx of macrophages and microglia are activated. Activation of microglia can be due to release of nucleotides (ADP and ATP) from the damaged cells into the extracellular matrix. Additionally, the infiltrating peripheral macrophages are also responsible, in part, in activating resident microglia (Wang et al., 2014). Once activated, microglia are critically involved in helping reseal the ruptured BBB (Lou et al., 2016). Upon activation, microglia retract their processes and typically adopt an amoeboid morphology (Csuka et al., 2000; Davalos et al., 2005; Smith, 2010). We have previously demonstrated that there is a significant increase in amoeboid microglia/macrophages after TBI in the dentate gyrus and thalamus (Bedi et al., 2013, 2013, 2018; Caplan et al., 2020). Additionally, in patients, the corpus callosum is surrounded by activated microglia (Johnson et al., 2013). Once activated, microglia can polarize towards a pro-inflammatory phenotype which can result in chronic neuroinflammation, oxidative stress and neuronal dysfunction. On the other hand, microglia can also be considered anti-inflammatory and can result in resolution of inflammation, clearance of debris and neural repair. The pro- or anti-inflammatory phenotype is dependent upon the local environment and timing after injury (Loane and Byrnes, 2010).

Another protein that increases in expression after injury is the translocator protein (TSPO), expressed by microglia, reactive astrocytes, blood-derived macrophages, endothelial and smooth muscle cells in the vasculature (Banati et al., 2000; Raghavendra Rao et al., 2000; Maeda et al., 2007; Rojas et al., 2007; Ji et al., 2008). TSPO or peripheral benzodiazepine receptor (PBR) is localized on the outer mitochondrial membranes of astrocytes, microglia and macrophages (Papadopoulos, 1998). TSPO or PBR can be detected in rodents and patients using positron emission topography (PET) ligands. Evidence from human TBI patients using ligand PK11195 (TSPO) suggests that amoeboid microglia/macrophages and/or reactive astrocytes remain present up to 17 years after injury (Ramlackhansingh et al., 2011). Second generation ligands with higher affinity and specificity for TSPO include PBR28 (Owen et al., 2011; Ching et al., 2012). However, binding of PBR28 is determined by genetic variation in the TSPO gene (Owen et al., 2012).

In order to determine if PET ligand for PBR (^{11}C-PBR28) is indeed a viable marker to measure activated microglia/macrophages, we utilized a multi-pronged in vivo (PET) and ex vivo (morphology and co-staining) approach. Elucidating the extent to which PBR28suv (in vivo analysis) is accompanied by amoeboid microglia (ex vivo analysis) and co-staining of PBR with microglia pre-clinically will allow us to advance the use of this ligand to assess the level of activated microglia after TBI or other CNS related neuroinflammatory diseases in clinic. In addition PBR28suv can serve as a biomarker for efficacy of cellular therapies that target neuroinflammation/microglia after TBI or stroke (Savitz and Cox, 2016).

Methods

Adult male Sprague Dawley rats aged six to eight weeks (Harlan/Envigo, Indianapolis, IN, USA) were housed on a twelve-hour light/dark cycle with ad libitum access to food and water. We used male rats because of our previous experiments and number of animals used was based on our previous publications (Bedi et al., 2013, 2013, 2018; Caplan et al., 2020). The sample size was also based on our previously published data and analysis (Bedi et al., 2018; Caplan et al., 2020). All protocols involving the use of animals were in compliance with the National Institutes of Health Guide for the Care and Use of Laboratory Animals and were approved by the Institutional Animal Care and Use Committee (HSC-AWC-15-0003).

CCI Model of Traumatic Brain Injury

Prior to creation of the TBI, each animal went through a pre-operative checklist to maximize survival following the controlled cortical impact (CCI). Each animal was initially anesthetized with 4% isoflurane with a 1:1 N_2O/O_2 mixture in a vented anesthesia chamber. When the animal failed to respond to foot and tail pinch, they were removed from the anesthesia chamber and continually anesthetized with a 2–2.5% isoflurane mixture via facemask. Aseptic surgical technique was used for the surgical procedure. Body temperature was monitored by a rectal thermometer and regulated by the use of a heating pad throughout the operation. Prior to any incision, the subcutaneous tissue was infiltrated with < 0.1 mL/kg of 0.25% Bupivacaine.

The CCI began with a midline scalp incision and the right-sided soft tissue was reflected laterally to expose the skull. Unilateral craniectomy was made midway between the bregma and the lambda (3 mm right of midline) with the medial edges adjacent to the midline suture. A single impact was performed using a sterile impactor tip. The scalp was then stapled closed with sterile wound clips.

In order to assess the spatial and temporal microglia response to injury, the rats were randomly selected to undergo either a sham injury or a right sided CCI (Device: Impact One Stereotaxic Impactor, Leica Microsystems, Buffalo Grove, IL). CCI severity is based on injury depth, and was measured independently by a device attached to the impactor tip (6 mm). The severe injury consisted of a 3.1 mm impact depth at a velocity of 5.6 m/s, dwell time 200 ms. The sham procedure entailed a midline incision and reflection of the soft tissue laterally to expose the skull. A craniectomy was not performed in this animal group. A traditional sham operation that incorporates craniectomy results in profound inflammatory and anatomical damage that may severely confound results of a TBI animal model, therefore it has become standard to not perform a craniectomy for sham procedures. This methodology has remained standard in our lab, which focuses primarily on rodent TBI models (Liao et al., 2014). Five animals (body weight 225-249 g) were assigned to each injury group.

Synthesis of [11C] PBR-28

The radioligand [11C] PBR-28 was purchased and synthesized from the University of Texas MD Anderson Cancer Center Cyclotron Radiochemistry Facility. In brief, [11C] CO_2 is produced in the cyclotron target by the bombardment with protons on nitrogen gas (N^{2+} 1% O_2) mixture via the nuclear reaction $^{14}N_{(p,\alpha)}^{11}C$. After irradiation, the [11C] CO2 from the target is transferred to a processing module where it is first trapped and then converted to [11C] methane. Subsequently, the [11C] methane is reacted to yield [11C] methyl iodide. The [11C] CH_3I is then passed through another column containing silver triflate at elevated temperatures, which in turn produces [11C] methyl triflate. The [11C] methyl triflate is then transferred to a second automated synthesis module where it reacts with the precursor. After the reaction, the solution is injected into a Prep HPLC column where the final product is purified. From this second module, the radiopharmaceutical is passed through a sterilizing filter into a sterile final product vial. A sample from the final product vial is removed and analyzed to ensure the product meets release criteria. Finally, the vial is moved to the radiopharmacy for individual dose dispensing.

PET/CT Imaging

Imaging was performed at the MD Anderson Cancer Center for Advanced Biomedical Imaging (CABI)/ Small Animal Imaging Facility (SAIF) 120 hours after creation of the injuries. A total of five rats with TBI were used for a dynamic ^{11}C-PBR28- PET/CT imaging study and an additional five rats were used as sham-treated controls. Rats were anesthetized using 2% isoflurane via facemask. At the start of the PET scan, the rats were injected with 300 uCi of ^{11}C-PBR28 in 200-μL of sterile saline via a tail vein catheter. Each rat was imaged with a sixty-minute PET scan and a five-minute CT scan (400 μA, 45 kV, 120 projections) on a Bruker Albira PET/SPECT/CT scanner (Bruker Biospin Corp., Billerica, MA, USA).

Imaging Data Analysis

The PET data was reconstructed into the following bins: 15×20 s, 5×60 s, and 4×300 s using a maximum likelihood expectation maximization (MLEM) method. Analysis was performed with P_{mod} (PMOD Technologies Ltd., Zürich, Switzerland). Using the skull outline from the CT image, two regions were drawn to cover the two cerebral hemispheres of the brain. The time-activity curve developed was [11C] PBR-28 Uptake in each region over the period of the PET scan was expressed as Standardized Uptake Values (SUV [g/ml]). This allows for body mass and minor variations in injected dose. Scatter, randoms, decay, and attenuation corrections were applied.

The SUV has become widely used in PET imaging analysis, making it an excellent tool for comparing radioligand uptake amongst our three different TBI injury severity groups. The SUVR is considered a semi-quantitative analysis defined as the ratio of tracer activity in the tissue of interest divided by normalizing tracer activity (background activity, organ activity, etc) (Thie, 2004). The regions of interest (ROIs) included: 1) the ipsilateral-injured cerebral hemisphere and 2) bilateral cerebral hemispheres to account for the contrecoup injury. Soft tissue uptake of the radioligand ^{11}C-PBR28 was excluded from analysis, so only intracranial microglia activation was evaluated. The SUV was determined by the ratio of mean intracranial SUVR to that of muscle. Contralateral brain hemisphere normalization was not possible, as contrecoup injuries would artificially lower mean SUVRs in the severe injury group.

Tissue Harvest and Immunohistochemistry

Approximately five hours after imaging, the animals were euthanized. The animals first underwent bilateral thoracotomies under isoflurane anesthesia. Then, using a right ventricle puncture technique, the animals were simultaneously exsanguinated and perfused with 20 mL of cold phosphate buffered saline (PBS). Following the PBS infusion, 20 mL of freshly prepared, cold 4% paraformaldehyde (PFA) was instilled to reduce non-specific binding and auto-fluorescence. The brains were carefully removed and post-fixed with 4% PFA for 24 hours while stored at 4°C. The brains were then transferred

to a 30% sucrose solution, where they were maintained at 4°C for at least 72 hours and allowed to sink. Brains were then put in a 3% melted agar mold and sectioned into 30-μm-thick slices using a vibrating-blade microtome (Leica Microsystems, Bannockburn, IL). A single histological section per animal approximately from mid-injury (interaural 5.70 mm, bregma − 3.30 mm) was examined.

Brain sections were stained for microglia using a free-floating protocol. The protocol was carried out over several days. On day one, the brain slices were transferred to twelve well plates and washed twice in PBS with 0.01% Triton X-100 (PBST; T-8787; Sigma-Aldrich, St. Louis,

MO) for 1 minute. Next, the slices were incubated for 20–30 minutes in PBS with 0.02% Triton X-100 for permeabilization. The slices were then blocked for one hour in blocking buffer consisting of 3% goat serum (no. 005-000-121; Jackson Immunoresearch Laboratories, West Grove, PA) in PBST. The last step of day one involved incubating the brain slices with the primary antibody IBA-1, which is used to identify microglia/macrophage morphology (rabbit polyclonal primary antibody, 1:500; Wako Chemicals USA, Cat# 019-19741, RRID: AB_2313566) (Bedi et al., 2013, 2013, 2018; Caplan et al., 2020). The primary antibody was prepared in PBTB (PBST, 2% bovine serum albumin [A9647;
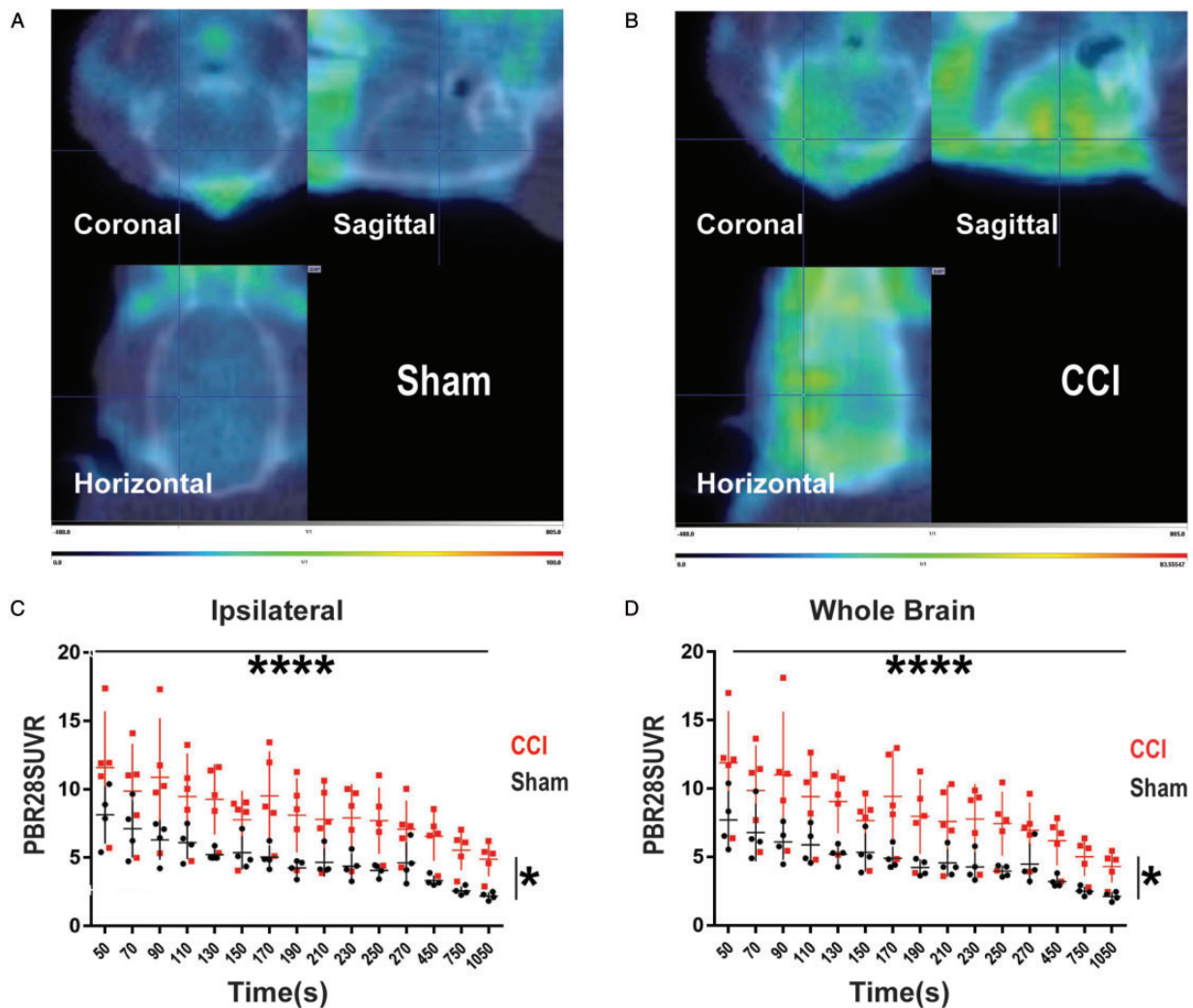

Figure 1. CCI Results in an Increase in the PBR28SUVR 5 Days After Injury. PET imaging was compared (5 days after CCI) between Sham and CCI. A: PET/CT image of a sham animal. Note the lack of red (PBR28) in the Sagittal and Horizontal views (B) PET/CT image of an injured animal 120 hours after a CCI. Note the greenish-yellow (PBR28) in the Coronal, Sagittal and Horizontal views. Extra-cranial soft tissue radioligand uptake was excluded from analysis. C: There were significant interaction of PBR28SUVR from 50 s to 1050 s ($p < 0.0001$, horizontal line), and there was an overall group difference between CCI and Sham ($p = 0.037$, vertical line) as measured by PBR28SUVR in the ipsilateral hemisphere (*: $p < 0.05$, ****: $p < 0.0001$) by 2-way ANOVA. D: There were significant interaction of PBR28suv from 50 s to 1050 s ($p < 0.0001$, horizontal line), and there was an overall group difference between CCI and Sham ($p = 0.036$, vertical line) as measured by PBR28SUVR in the whole brain (*: $p < 0.05$, ****: $p < 0.0001$) by 2-way ANOVA. Cross hairs indicate site of injury.

Sigma-Aldrich] and 1% goat serum), and sections were incubated overnight at 4°C. The following day, sections were washed with PBST and incubated with a goat anti-rabbit IgG secondary antibody (1:500; red/568; Molecular Probes (Invitrogen) Cat# A11011, RRID: AB143157) in PBTB for 2 hours at room temperature. The sections were again rinsed four times with PBST, mounted on slides, and cover-slipped with Fluoromount-G (SouthernBiotech) for analysis.

Microglia Morphology Quantification. *Ex vivo* analysis in CCI and sham was done by quantifying microglia morphology with photomicrographs of the injury penumbra, dentate gyrus (hippocampus), thalamus (lateral and medial) and corpus callosum. Photomicrographs were taken at 20X magnification using a Leica fluorescent microscope Dm4000B LED (https://www.leica-microsystems.com/products/light-microscopes/p/leica-dm4000-b-led) and Leica Application Suite V4.12 (https://www.leica-micro systems.com/products/microscope-software/p/leica-appli cation-suite). A single slice per animal was examined and the sections of interest were approximately mid-injury (small cavity or bruise left by the impactor tip). IBA-1 labeled cells were further quantified based on the following microglia morphologies: ramified or amoeboid as previously described (Bedi et al., 2013, p. 429; Torres-Platas et al., 2014).

Co-Staining of IBA1/PBR and GFAP/PBR

A single brain section from each animal of each was group were co-stained with IBA1 and PBR. In addition, we also co-stained glial fibrillary acidic protein (GFAP) and PBR. Primary antibodies included: Anti-PBR (goat polyclonal primary antibody, 1:50; Abcam Cat# ab118913, RRID: AB_10898989), GFAP (rabbit poly-clonal antibody, 1:500; Abcam Cat# ab7260, RRID:

AB_305808), and IBA-1 (rabbit polyclonal primary anti-body, 1:500; Wako Chemicals USA, Cat# 019-19741, RRID: AB_2313566). Secondary fluorescent antibody products included: Alexa Fluor® 488 (donkey polyclonal secondary antibody to rabbit IgG H&L, 1:500; Abcam Cat# ab150073, RRID: AB_2636877) and Alexa Fluor® 568 (donkey polyclonal secondary antibody to goat IgG H&L, 1:500; Abcam Cat# ab175704). Antibody staining combinations included: IBA1/PBR and GFAP/PBR. All photomicrographs were taken blinded and the analyses were done blinded as well.

Statistical Analysis

All data are expressed as means ± standard deviation. Statistical analysis was performed with Prism software (version 7.0 b; GraphPad Software Inc., La Jolla, CA). *In vivo* SUV were analyzed with Two-way analysis of variance (ANOVA) was used for data comparison between Sham vs CCI for the PBR28SUVR. Area under curve analysis and correlation analysis was done by Prism software. *Ex vivo* microglia cell counts were compared using unpaired non parametric Mann-Whitney test. Outliers were excluded using ROUT with $Q = 1\%$. Statistical significance is indicated with * for $p < 0.05$, ** indicates statistical significance for $p < 0.01$, *** indicates statistical significance $p < 0.001$, and **** indicates statistical significance $p < 0.0001$.

Results

CCI Increases PBR28suv in Experimental TBI Model

Representative PET images are displayed in Figure 1A and B. The time-activity curves of the ipsilateral hemisphere demonstrates that there is an increase in PBR28suv after a brain injury. When comparing the PBR28SUVR (ipsilateral) over time, there was a significant increase in
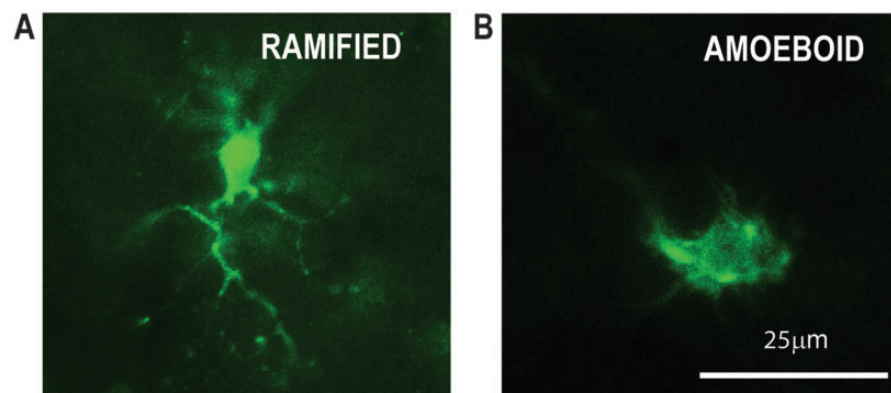

Figure 2. The Different Morphological Phenotypes of Microglia/Macrophages Using IBA1. A: The non-activated have a small cell body, with extensive, fine branching processes. B: The activated demonstrate very short processes and a condensed amoeboid-shape. Scale bar 25 μm.

PBR28suv—$F_{(14,98)}=20.2$, $P < 0.0001$, Figure 1C. In addition, there was a difference between sham and CCI—$F_{(1,7)}=6.59$, $P = 0.037$, Figure 1C. The whole brain PBR28SUVR demonstrated similar changes over time—$F_{(14,98)}=21.6$, $P < 0.0001$, Figure 1D. Additionally, there was a significant difference between sham and CCI—$F_{(1,7)}=6.65$, $P = 0.036$, Figure 1D. From 50 s to 1050 s, CCI animals have a higher SUV than sham. [^{11}C]PBR28 uptake is relatively stable over the course of the imaging.

CCI Results in an Increase in Amoeboid Microglia/Macrophages in the Ipsilateral Injury Penumbra

Controlled cortical impact resulted in a significant decrease of ramified IBA1 positive cells in the penumbra of the injury. Injured animals had (Figure 3A and C, $p = 0.016$) a significantly lower number (CCI: n = 5, 0.2 ± 0.4) of ramified IBA1+ cells (Figure 2A) when compared to sham (n = 4, 19.7 ± 2.5). Controlled cortical impact also resulted in a significant increase of amoeboid
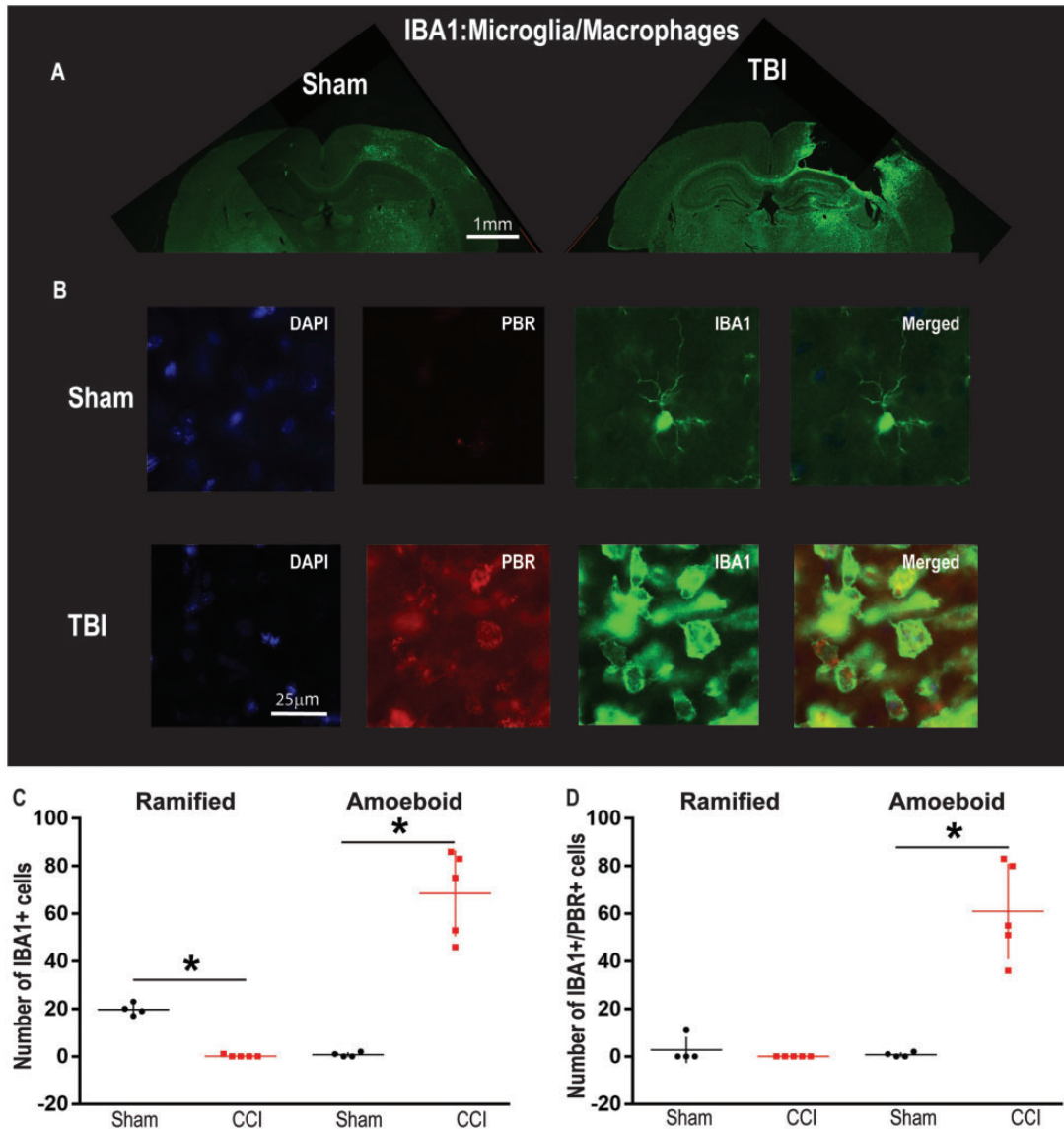

Figure 3. CCI Results in an Increase in the Number of Amoeboid IBA1 Positive Cells in the Ipsilateral Injury Penumbra 5 Days After Injury. A: Whole brain photomicrographs (1.25×) of Sham and CCI with IBA1 antibody. Note the increase in fluorescence in the CCI photomicrograph in comparison to Sham. Scale bar 1 mm. B: There is a lack of co-staining of PBR with ramified (sham) IBA1 positive cells (merged) in comparison to amoeboid (CCI) IBA1 positive cells (merged). Note the increase in PBR (red) in CCI in comparison to Sham. Scale bar 25 μm. C: Ipsilateral to the injury, CCI significantly increased the number of amoeboid IBA1 positive cells in comparison to sham and significantly decreased the ramified cells in CCI (*: $p < 0.05$) by unpaired non parametric Mann-Whitney test. D: CCI significantly increased the number of amoeboid IBA1/PBR positive cells in comparison to sham.
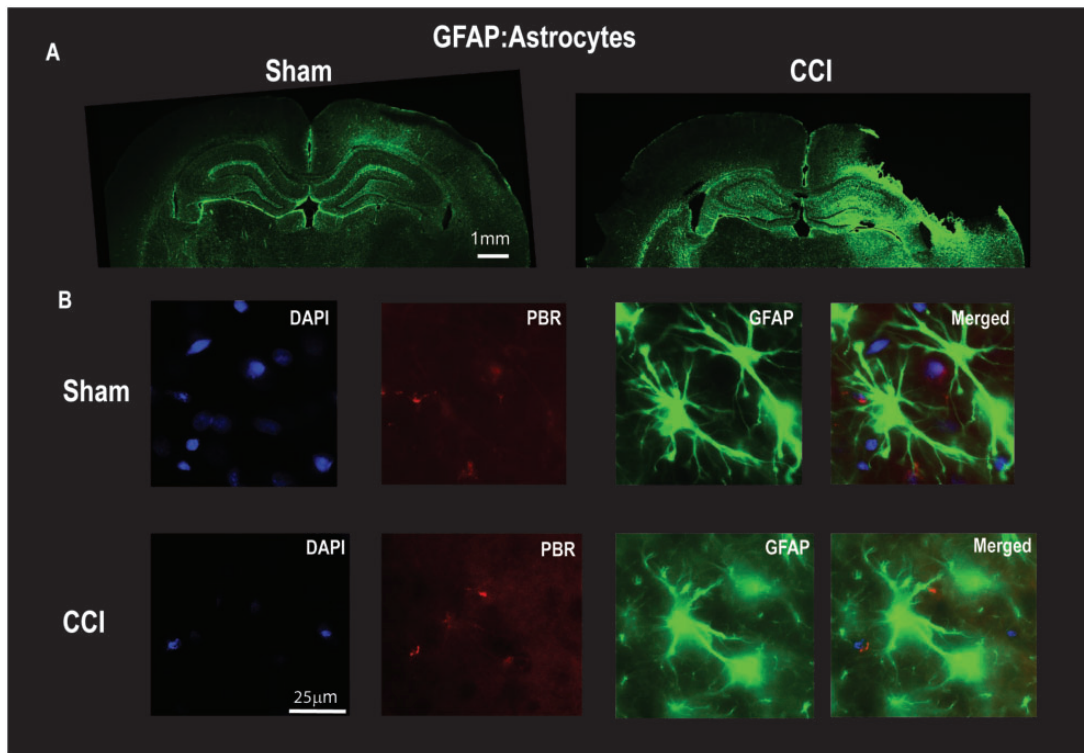
Figure 4. CCI Results in an Increase in the Number of GFAP Positive Cells in Injury Penumbra 5 Days After Injury. A: Whole brain photomicrographs (1.25×) of Sham and CCI with GFAP antibody. Note the increase in fluorescence in the CCI photomicrograph in comparison to Sham. Scale bar 1 mm. B: There is an overall lack of co-staining of PBR with GFAP positive cells in either groups (Sham or CCI). Scale bar: 25 µm.

IBA1 positive cells in the penumbra of the injury. Injured animals had (Figure 3C, p = 0.016), a significantly lower number (CCI: n = 5, 68.6 ± 18) amoeboid IBA1 positive cells (Figure 2B) when compared to sham (n = 4, 0.75 ± 0.95). Similar to increase in PBR28 SUVR observed in vivo (Figure 1A and B), there was a significant increase in co-staining of IBA1 positive cells with PBR. Specifically, there was a significant increase in the amoeboid IBA1+ cells that co-stained for PBR (IBA1/PBR) in the CCI group [CCI: n = 5, 61 ± 20 vs Sham: n = 4, 0.75 ± 0.95 (Figure 3D, p = 0.016)]. However, there was no significant differences in the "Ramified" IBA1+/PBR group between CCI and Sham. (p = 0.4). Surprisingly, we did not observe any co-staining of GFAP and PBR (Figure 4A to D). While there was an increase in GFAP staining (not quantified, Figure 4A) between Sham and TBI, we did see any overlap between GFAP and PBR (Figure 4B).

Correlation between PBR28suv (ipsilateral: Area under Curve) and amoeboid IBA1 positive cells was not significant (p = 0.78 and Spearman r = 0.2, graph not shown) for CCI (Area under curve: 61.5) and Sham (Area under curve: 54.4, p = 0.67, Spearman r = 0.5, graph not shown).

CCI Results in an Increase in Amoeboid Microglia/Macrophages in the Ipsilateral Corpus Callosum

Controlled cortical impact resulted in a significant increase in amoeboid IBA1 positive cells in the corpus callosum. Specifically, there was an increase in the amoeboid microglia/macrophages ipsilateral to the injury (Figure 5B, p = 0.029, n = 4, 102 ± 13) when compared to sham (n = 4, 3.75 ± 4.2), but not contralateral to the injury [CCI: n = 5, 10.8 ± 13 vs Sham: n = 4, 5.00 ± 3.9 (Figure 5B, p = 0.13)]. Interestingly, there were no differences in the number of ramified microglia/macrophages on either the ipsilateral—Figure 5A, CCI: n = 5, 274 ± 90 vs Sham: n = 4, 136 ± 12 (p = 0.11)—or contralateral hemisphere—Figure 5B, CCI: n = 4, 142 ± 6.8 vs Sham: n = 4, 134 ± 18 (p = 0.34).

CCI Results in an Increase in Amoeboid Microglia/Macrophages Ipsilateral to the Injury in the Dentate Gyrus

Controlled cortical impact resulted in a significant increase in amoeboid IBA1 positive cells in the ipsilateral dentate gyrus only—Figure 6B, CCI: n = 5, 91.2 ± 97 vs
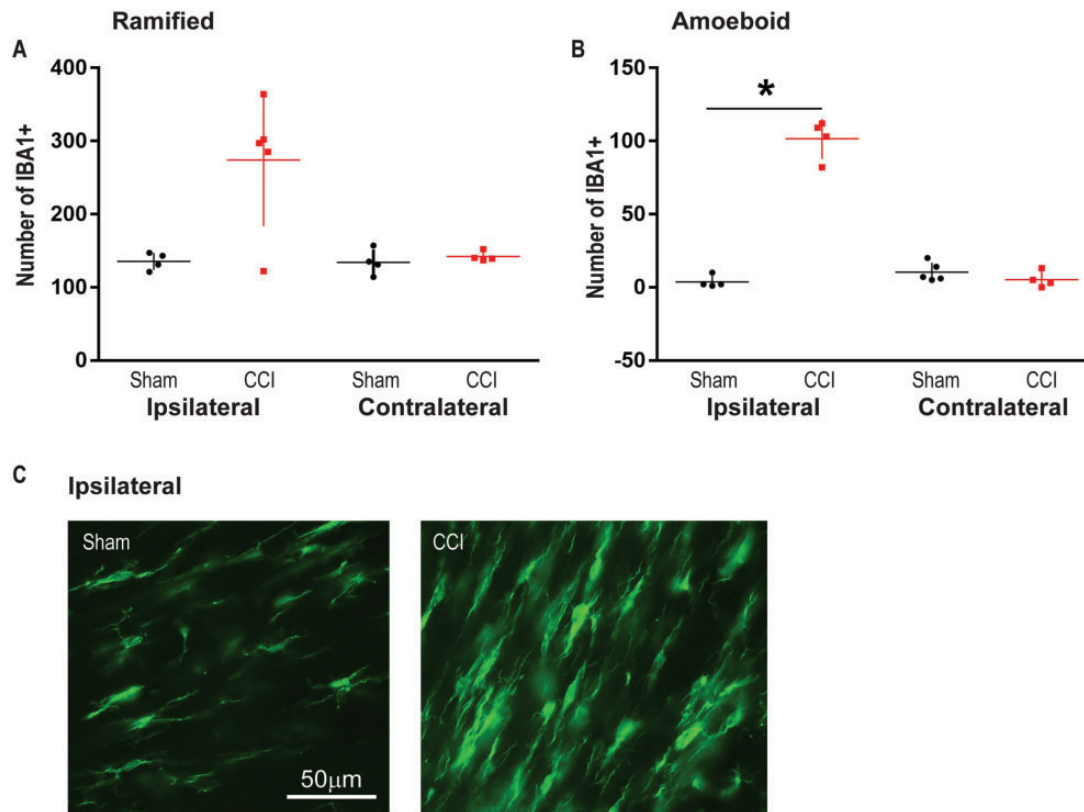
Figure 5. CCI Results in an Increase in the Number of Amoeboid Shaped IBA1 Positive Cells in The Ipsilateral Corpus Callosum 5 Days After Injury. A: CCI modestly increased the number of ramified cells in comparison to sham (ipsilateral and contralateral) but this was not significant. B: Ipsilateral to the injury, CCI significantly increased the number of amoeboid shaped IBA1 positive cells in comparison to sham (*: $p < 0.05$) by unpaired non parametric Mann-Whitney test. There was no change in the contralateral side. C: Photomicrographs of ramified (Sham) and amoeboid (CCI) microglia.

Sham: n = 4, 4.25 ± 2.2 (p = 0.016). There was no increase in the number of amoeboid IBA1 positive cells contralateral to the injury—Figure 6B, CCI: n = 5, 10.8 ± 13 vs Sham: n = 4, 5.00 ± 3.9 (p = 0.63)—when compared to sham. There were no differences in the number of ramified microglia in the ipsilateral— Figure 6A, CCI: n = 5.00, 158 ± 95 vs Sham: n = 4, 135 ± 12 (p = 0.60)—or contralateral hemisphere— Figure 6A, CCI: n = 5, 143 ± 47 vs Sham: n = 4, 134 ± 18 (p = 0.99)—when compared to sham.

CCI Results in an Increase in Amoeboid Microglia/ Macrophages in the Medial Ipsilateral Thalamus

Controlled cortical impact resulted in a significant increase in amoeboid IBA1 positive cells in the medial ipsilateral thalamus when compared to sham— Figure 7B, CCI:n = 5, 50.2 ± 21 vs Sham: n = 4, 9.00 ± 7.1 (p = 0.016). There were no differences in the contralateral side when compared to sham—Figure 7B, CCI : n = 4, 8.50 ± 15 vs Sham: n = 3, 1.00 ± 0.0 (p = 0.99). Additionally, there were no differences in the number

of ramified IBA1 positive cells ipsilaterally—Figure 7A, CCI: n = 5, 38.2 ± 13 vs Sham: n = 4, 28.0 ± 5.7 (p = 0.34)—and contralaterally—Figure 7A, CCI: n = 4, 21.5 ± 13 vs Sham: n = 4, 36.0 ± 8.4 (p = 0.17)—when compared to sham.

CCI Results in an Increase in Amoeboid Microglia/ Macrophages in the Lateral Ipsilateral Thalamus

Similar to the medial thalamus, CCI resulted in a significant increase in amoeboid IBA1 positive cells in the lateral ipsilateral thalamus when compared to sham— Figure 8B, CCI: n = 5, 69.6 ± 34 vs Sham: n = 4, 7.00 ± 7.2 (p = 0.016). There were no differences in the contralateral side when compared to sham—Figure 8B, CCI: n = 5, 13.0 ± 14 vs Sham: n = 4, 2.00 ± 2.7 (p = 0.11). Also, there were no differences in the number of ramified microglia/macrophages on either the ipsilateral— Figure 8A, CCI: n = 5, 35.4 ± 16 vs Sham: n = 4, 24.0 ± 7.8 (p = 0.31)—or contralateral hemisphere—Figure 8A, CCI: n = 5, 27.8 ± 17 vs Sham: n = 4, 22.5 ± 17 (p = 0.37)—when compared to sham.
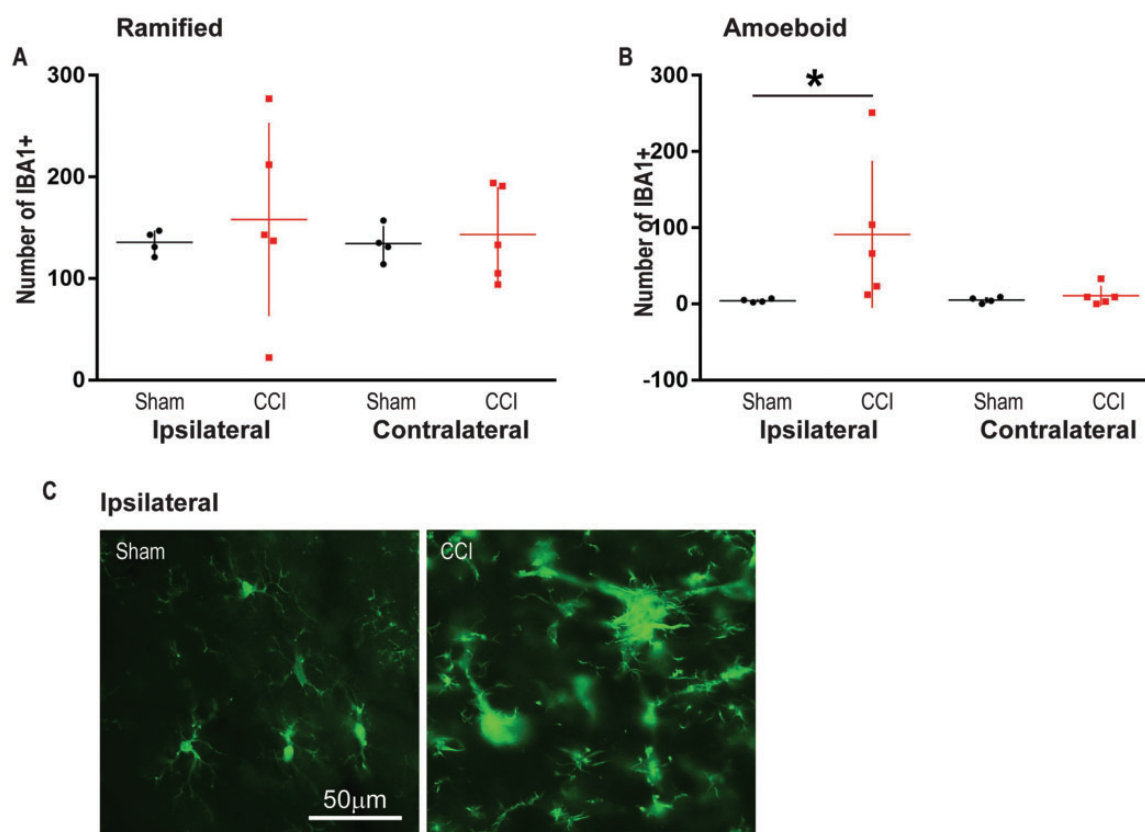
Figure 6. CCI Results in an Increase in the Number of Amoeboid Shaped IBA1 Positive Cells in the Ipsilateral Dentate Gyrus 5 Days After Injury. A: There was no increase due to CCI in the number of ramified cells in comparison to sham (ipsilateral and contralateral). B: Ipsilateral to the injury, CCI significantly increased the number of amoeboid shaped IBA1 positive cells in comparison to sham (*: $p < 0.05$) by unpaired non parametric Mann-Whitney test. There was no change in the contralateral side. C: Photomicrographs of ramified (Sham) and amoeboid (CCI) microglia. Scale bar: 50 μm.

Discussion

Our results demonstrate that 11C-PBR28 PET can quantitatively detect enahanced microglial activation followingbrain injury *in vivo* in a rodent model of TBI. These data are translationally relevant as activated microglia are being explored as therapeutic targets after TBI and stroke (Savitz and Cox, 2016). Traumatic brain injury can be studied in laboratory setting via a number of different models which include CCI, weight drop injury (WDI), fluid percussion injury (FPI) and blast-induced TBI (bTBI). We have used CCI (pneumatic and electromagnetic) to induce a reproducible and well-controlled injury (Lighthall, 1988). CCI provides control over the depth of injury, velocity, tip size and dwell time of the injury. All these variables can be successfully reproduced in an experimental setting. CCI, with a 3.1 mm depth, 200 ms dwell time and 5.6 m/s velocity resulted in a significant increase in PBR28SUVR in the ipsilateral and bilateral hemispheres (Figure 1). The increase in uptake is accompanied by significant increases in amoeboid microglia/macrophages that are IBA1 positive in the ipsilateral injury penumbra, corpus callosum,

dentate gyrus, medial thalamus and lateral thalamus (Figures 3 and 5 to 8). Surprisingly, the correlation between SUV (area under the curve) and amoeboid IBA1 positive cells in the ipsilateral injury penumbra is not significant (graph not shown).

In vivo PET imaging allows us to assess the extent of immune activation. TSPO/PBR, an often PET-imaged protein is upregulated after injury (Maeda et al., 2007, p. 288; Raghavendra Rao et al., 2000). Recent evidence from Pannell et al. (2020) demonstrated that TSPO is upregulated in astrocytes and microglia when stimulated with lipopolysaccharide (LPS), and this is reflected with an increase in PET imaging of TSPO ligand ^{18}F-DPA-713 (Pannell et al., 2020). In addition, they demonstrated TSPO expression was significantly increased in microglia after AdTNF injections (Pannell et al., 2020). These data indicate that TSPO is a good marker to target in order to observe increases of pro-inflammatory microglia *in vivo*. *Ex vivo*, we have previously utilized morphology to delineate between activated and resting microglia after TBI (Bedi et al., 2013, 2018). Microglia are activated after a CNS injury. They retract their processes and adopt an amoeboid morphology
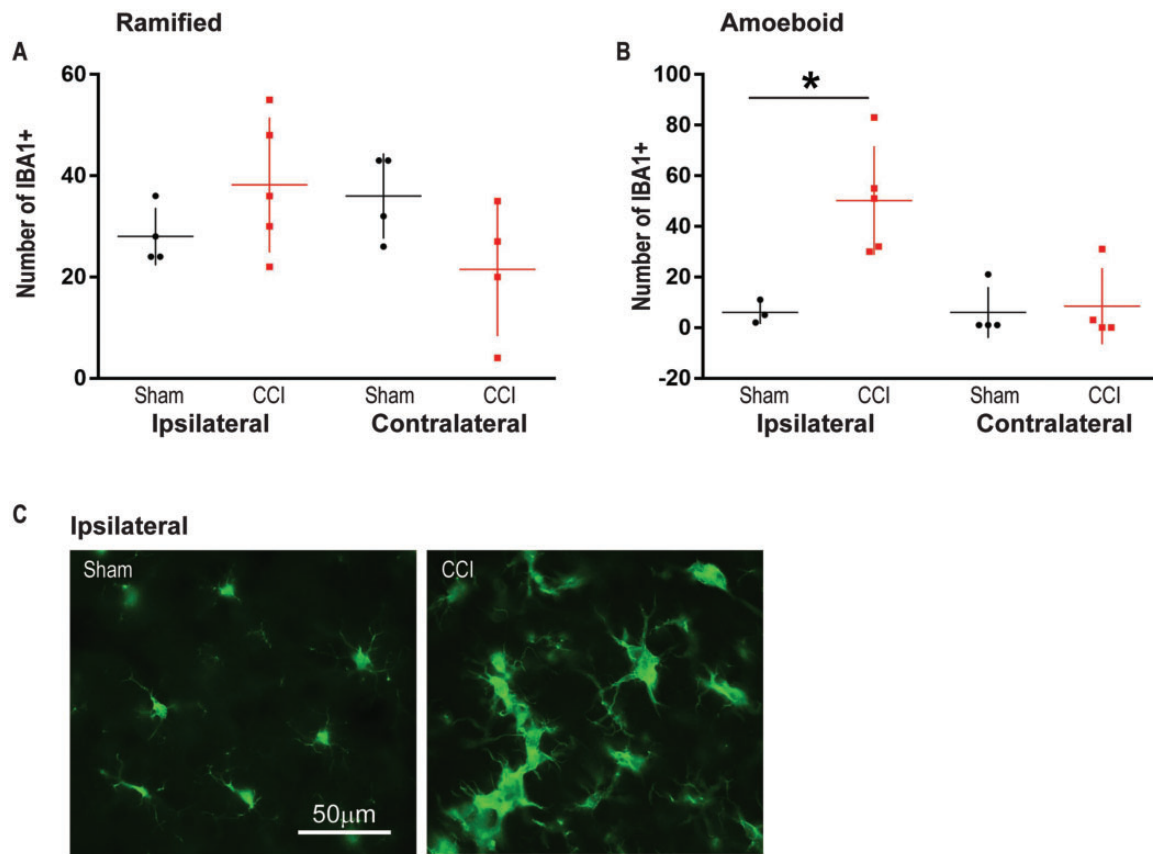
Figure 7. CCI Results in an Increase in the Number of Amoeboid Shaped IBA1 Positive Cells in the Ipsilateral Medial Thalamus 5 Days After Injury. A: There was no increase due to CCI in the number of ramified cells in comparison to sham (ipsilateral and contralateral). B: Ipsilateral to the injury, CCI significantly increased the number of amoeboid shaped IBA1 positive cells in comparison to sham (*: $p < 0.05$) by unpaired non parametric Mann-Whitney test. There was no change in the contralateral side. C: Photomicrographs of ramified (Sham) and amoeboid (CCI) microglia. Scale bar: 50 μm.

(Csuka et al., 2000; Davalos et al., 2005; Smith, 2010; Bedi et al., 2013, 2018). Microglia are responsible for clearance of dead cells and other debris, such as dead axons and myelin and, therefore, have a neuroprotective role (Kalla et al., 2001), however, chronic activation of microglia can negatively affect neuronal function and hippocampal dependent behavior (Belarbi et al., 2012; Bedi et al., 2013; Hernandez-Ontiveros et al., 2013). In current experiments, in addition to an increase in PBR28SUVR, we also found increases in the number of amoeboid shaped in varying regions of the brain after TBI. In the injury penumbra (Figure 3), we observed a significant increase in amoeboid IBA1 positive cells (Figure 3C) that co-stained with PBR (Figure 3D), and this was limited amoeboid shaped cells (Figure 3B). Surprisingly, there was no correlation between PBR28SUVR (*in vivo*) and *ex vivo* analysis (graph not shown). Perhaps an increase in the number of animals sampled is required for appropriate correlation analysis. We also qualitatively examined co-staining of PBR with

GFAP. This was done in order to determine whether PBR28 is expressed in astrocytes after CCI. There was little to no co-staining of PBR and GFAP in either sham or CCI (Figure 4B).

Additionally, there was an increase in amoeboid shaped IBA1 positive cells in the ipsilateral corpus callosum (Figure 5). Previously, case analysis of patients that suffered TBI showed presence of activated microglia with white matter degeneration ranging from months to 47 years. Specifically, there was a reduction in corpus callosum thickness surrounded by activated microglia (Johnson et al., 2013). We observed an increase the number of amoeboid microglia/macrophages in the ipsilateral corpus callosum only (Figure 5). There was a very modest increase on the contralateral side but it was not significant (Figure 5A and B). In addition to the ipsilateral corpus callosum, there were significant increases in amoeboid microglia in the ipsilateral dentate gyrus of the hippocampus (Figure 6) and the ipsilateral lateral and medial thalamus (Figures 7 and 8). Both areas have
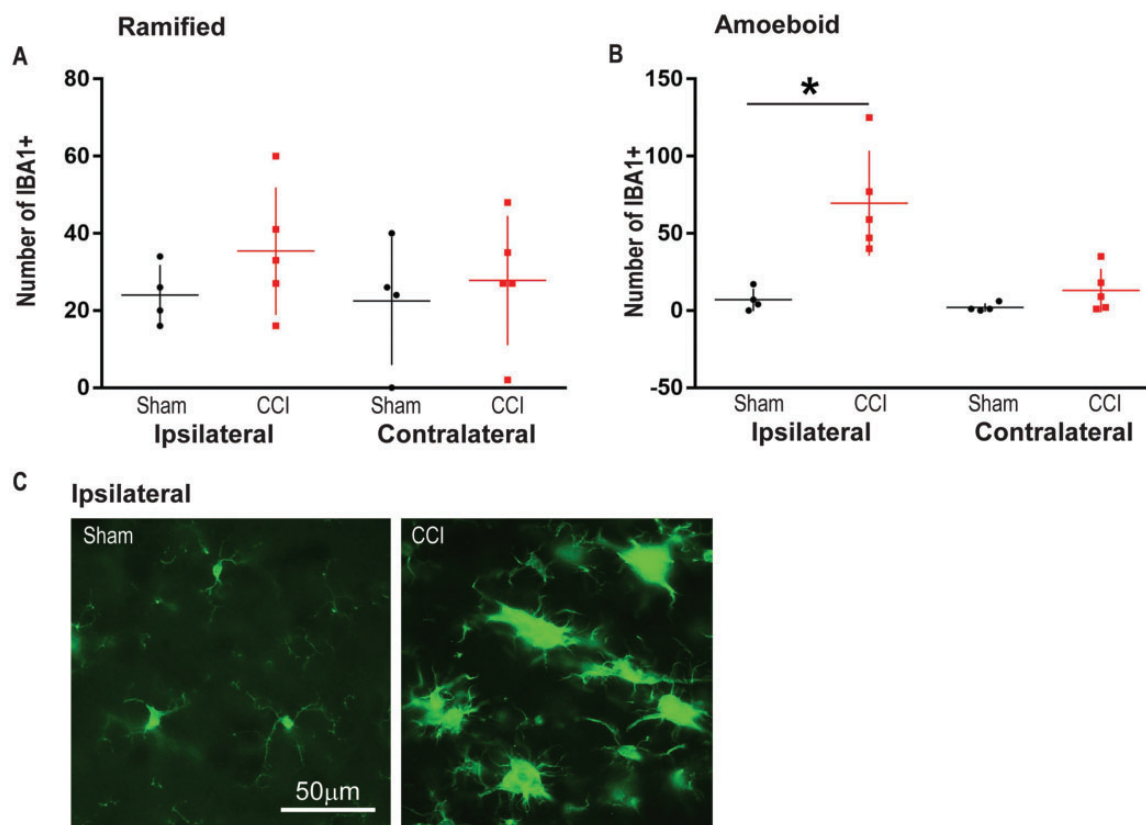
Figure 8. CCI Results in an Increase in the Number of Amoeboid Shaped IBA1 Positive Cells in the Ipsilateral Lateral Thalamus 5 Days After Injury. A: There was no increase due to CCI in the number of ramified cells in comparison to sham (ipsilateral and contralateral). B: Ipsilateral to the injury, CCI significantly increased the number of amoeboid shaped IBA1 positive cells in comparison to sham (*: $p < 0.05$) by unpaired non parametric Mann-Whitney test. There was no change in the contralateral side. C: Photomicrographs of ramified (Sham) and amoeboid (CCI) microglia. Scale bar: 50 μm.

previously demonstrated increases in amoeboid shaped microglia after CCI (Bedi et al., 2013; Caplan et al., 2020).

Amoeboid shaped microglia have also been observed as early as 7 days and up to 28 days after injury in the ventral posteromedial nucleus of the thalamus using FPI (Thomas et al., 2018). Studies have linked TBI and increased activity in the ipsilateral auditory thalamus (medial geniculate nucleus) to a fear conditioning paradigm (amygdala) (Hoffman et al., 2019). The dentate gyrus is an area in the hippocampus that is critical for spatial learning after TBI (Bedi et al., 2018). The lack of increase in the contralateral (Figure 6) was surprising since previously we had previously observed increases in the contralateral side as well just 24 hours after injury. However those experiments were conducted in mice (Caplan et al., 2020).

Our results indicate that TBI results in an increase in PBR28suv, an indicator of activated microglia/macrophages (Pannell et al., 2020). Furthermore, ex *vivo* analysis demonstrated increases in amoeboid (activated) microglia in the injury penumbra, corpus callosum,

dentate gyrus, lateral thalamus and medial thalamus as measured by immunohistochemistry. A possible limitation to this study is the reliance of microglia, as it is well understood that the secondary injury from TBI is a result of a complex inflammatory response that involves the activation and proliferation of peripheral immune cells such as blood-derived macrophages, T lymphocytes, natural killer cells, neutrophils, etc. Perhaps by eliminating blood-derived macrophages, we can discern and image microglia only after TBI (Aertker et al., 2019). Additional challenges in TSPO-PET imaging is the distinction between pro and anti-inflammatory microglia. Purinergic receptor (P2X7) is a likely target for pro-inflammatory microglia and metabotropic purinergic receptor (P2Y12) might be a target for anti-inflammatory microglia (Beaino et al., 2017). Development of these two radioligands might provide more detailed assessment of microglial contribution to neuroinflammation after TBI.

These experiments demonstrated the feasibility and limitations of utilizing PBR28suv based on injury vs sham in a small cohort of animals. However, a larger

sample size, chronic time points and male vs female are the next step in exploring this potential diagnostic tool. Traumatic brain injury results in a neuroinflammatory response marked by activated microglia/macrophages. While these cells may help at the site of injury by clearing damaged tissue, their chronic activation contributes to worsening secondary brain injury. PET/CT imaging studies would allow clinicians to track the neuroinflammatory response to different therapeutics.

Conclusion

PBR28suv has been a useful ligand that allowed visualization of activated microglia *in vivo* among several neurodegenerative diseases (Dupont et al., 2017). ^{11}C-PBR28 may be a promising tracer for monitoring neuroinflammation in TBI. Longitudinally, our study was able to confirm the feasibility of utilizing PET/CT imaging in discriminating between TBI and sham by demonstrating an injury-dependent increase in PBR28SUVR. In addition, we demonstrated that there is an ipsilateral increase in amoeboid shaped microglia/macrophages, and that PBR is present in amoeboid microglia/macrophages and not astrocytes.

Declaration of Conflicting Interests

Funding

ORCID iDs

Fanni Cardenas (ID) https://orcid.org/0000-0002-2026-5351
Franciska Gudenkauf (ID) https://orcid.org/0000-0002-7463-8934
Supinder S. Bedi (ID) https://orcid.org/0000-0003-1938-1790

References

Aertker, B. M., Kumar, A., Prabhakara, K. S., Smith, P., Furman, N. E. T., Hasen, X., Cox, C. S., & Bedi, S. S. (2019). Pre-injury monocyte/macrophage depletion results in increased blood-brain barrier permeability after traumatic brain injury. *Journal of Neuroscience Research*, *97*(6), 698–707. https://doi.org/10.1002/jnr.24395

Banati, R. B., Newcombe, J., Gunn, R. N., Cagnin, A., Turkheimer, F., Heppner, F., Price, G., Wegner, F., Giovannoni, G., Miller, D. H., Perkin, G. D., Smith, T., Hewson, A. K., Bydder, G., Kreutzberg, G. W., Jones, T.,

Cuzner, M. L., & Myers, R. (2000). The peripheral benzodiazepine binding site in the brain in multiple sclerosis: Quantitative in vivo imaging of microglia as a measure of disease activity. *Brain*, *123*(Pt 11), 2321–2337. https://doi.org/10.1093/brain/123.11.2321

Beaino, W., Janssen, B., Kooij, G., van der Pol, S. M., van Het Hof, B., van Horssen, J., Windhorst, A. D., & de Vries, H. E. (2017). Purinergic receptors P2Y12R and P2X7R: Potential targets for PET imaging of microglia phenotypes in multiple sclerosis. *Journal of Neuroinflammation*, *14*(1), 259. https://doi.org/10.1186/s12974-017-1034-z

Bedi, S. S, Aertker, B. M., Liao, G. P., Caplan, H. W., Bhattarai, D., Mandy, F., Mandy, F., Fernandez, L. G., Zelnick, P., Mitchell, M. B., Schiffer, W., Johnson, M., Denson, E., Prabhakara, K., Xue, H., Smith, P., Uray, K., Olson, S. D., Mays, R. W., & Cox, C. S., Jr. (2018). Therapeutic time window of multipotent adult progenitor therapy after traumatic brain injury. *Journal of Neuroinflammation*, *15*(1), 84. https://doi.org/10.1186/s12974-018-1122-8

Bedi, S. S., Hetz, R., Thomas, C., Smith, P., Olsen, A. B., Williams, S., Xue, H., Aroom, K., Uray, K., Hamilton, J., Mays, R. W., & Cox, C. S., Jr. (2013). Intravenous multipotent adult progenitor cell therapy attenuates activated microglial/macrophage response and improves spatial learning after traumatic brain injury. *Stem Cells Translational Medicine*, *2*(12), 953–960. https://doi.org/10.5966/sctm.2013-0100

Bedi, S. S., Walker, P. A., Shah, S. K., Jimenez, F., Thomas, C. P., Smith, P., Hetz, R. A., Xue, H., Pati, S., Dash, P. K., & Cox, C. S., Jr. (2013). Autologous bone marrow mononuclear cells therapy attenuates activated microglial/macrophage response and improves spatial learning after traumatic brain injury. *The Journal of Trauma and Acute Care Surgery*, *75*(3), 410–416. https://doi.org/10.1097/TA.0b013e31829617c6

Belarbi, K., Arellano, C., Ferguson, R., Jopson, T., & Rosi, S. (2012). Chronic neuroinflammation impacts the recruitment of adult-born neurons into behaviorally relevant hippocampal networks. *Brain, Behavior, and Immunity*, *26*(1), 18–23. https://doi.org/10.1016/j.bbi.2011.07.225

Caplan, H. W., Cardenas, F., Gudenkauf, F., Zelnick, P., Xue, H., Cox, C. S., & Bedi, S. S. (2020). Spatiotemporal distribution of microglia after traumatic brain injury in male mice. *ASN Neuro*, *12*, 1759091420911770. https://doi.org/10.1177/1759091420911770

Ching, A. S., Kuhnast, B., Damont, A., Roeda, D., Tavitian, B., & Dolle, F. (2012). Current paradigm of the 18-kDa translocator protein (TSPO) as a molecular target for PET imaging in neuroinflammation and neurodegenerative diseases. *Insights Imaging*, *3*(1), 111–119. https://doi.org/10.1007/s13244-011-0128-x

Csuka, E., Hans, V. H., Ammann, E., Trentz, O., Kossmann, T., & Morganti-Kossmann, M. C. (2000). Cell activation and inflammatory response following traumatic axonal injury in the rat. *Neuroreport*, *11*(11), 2587–2590.

Davalos, D., Grutzendler, J., Yang, G., Kim, J. V., Zuo, Y., Jung, S., Littman, D. R., Dustin, M. L., & Gan, W. B. (2005). ATP mediates rapid microglial response to local

brain injury in vivo. *Nature Neuroscience*, 8(6), 752–758. https://doi.org/10.1038/nn1472

Dupont, A. C., Largeau, B., Santiago Ribeiro, M. J., Guilloteau, D., Tronel, C., & Arlicot, N. (2017). Translocator protein-18 kDa (TSPO) positron emission tomography (PET) imaging and its clinical impact in neurodegenerative diseases. *International Journal of Molecular Sciences*, 18(4), 785. https://doi.org/10.3390/ijms18040785

Graeber, M. B. (2010). Changing face of microglia. *Science*, 330(6005), 783–788. https://doi.org/330/6005/783 [pii]10.1126/science.1190929

Hernandez-Ontiveros, D. G., Tajiri, N., Acosta, S., Giunta, B., Tan, J., & Borlongan, C. V. (2013). Microglia activation as a biomarker for traumatic brain injury. *Frontiers in Neurology*, 4, 30. https://doi.org/10.3389/fneur.2013.00030

Hoffman, A. N., Lam, J., Hovda, D. A., Giza, C. C., & Fanselow, M. S. (2019). Sensory sensitivity as a link between concussive traumatic brain injury and PTSD. *Scientific Reports*, 9(1), 13841. https://doi.org/10.1038/s41598-019-50312-y

Ji, B., Maeda, J., Sawada, M., Ono, M., Okauchi, T., Inaji, M., Zhang, M. R., Suzuki, K., Ando, K., Staufenbiel, M., Trojanowski, J. Q., Lee, V. M. Y., Higuchi, M., & Suhara, T. (2008). Imaging of peripheral benzodiazepine receptor expression as biomarkers of detrimental versus beneficial glial responses in mouse models of Alzheimer's and other CNS pathologies. *Journal of Neuroscience*, 28(47), 12255–12267. https://doi.org/10.1523/JNEUROSCI.2312-08.2008

Johnson, V. E., Stewart, J. E., Begbie, F. D., Trojanowski, J. Q., Smith, D. H., & Stewart, W. (2013). Inflammation and white matter degeneration persist for years after a single traumatic brain injury. *Brain*, 136(1), 28–42. https://doi.org/aws322 [pii]10.1093/brain/aws322

Kalla, R., Liu, Z., Xu, S., Koppius, A., Imai, Y., Kloss, C. U., Kohsaka, S., Gschwendtner, A., Möller, J. C., Werner, A., & Raivich, G. (2001). Microglia and the early phase of immune surveillance in the axotomized facial motor nucleus: Impaired microglial activation and lymphocyte recruitment but no effect on neuronal survival or axonal regeneration in macrophage-colony stimulating factor-deficient mice. *Journal of Comparative Neurology*, 436(2), 182–201.

Liao, G. P., Olson, S. D., Kota, D. J., Hetz, R. A., Smith, P., Bedi, S., & Cox, C. S., Jr. (2014). Far-red tracer analysis of traumatic cerebrovascular permeability. *Journal of Surgical Research*, 190(2), 628–633. https://doi.org/10.1016/j.jss.2014.05.011

Lighthall, J. W. (1988). Controlled cortical impact: A new experimental brain injury model. *Journal of Neurotrauma*, 5(1), 1–15.

Loane, D. J., & Byrnes, K. R. (2010). Role of microglia in neurotrauma. *Neurotherapeutics*, 7(4), 366–377. https://doi.org/S1933-7213(10)00088-7 [pii]10.1016/j.nurt.2010.07.002

Lou, N., Takano, T., Pei, Y., Xavier, A. L., Goldman, S. A., & Nedergaard, M. (2016). Purinergic receptor P2RY12-dependent microglial closure of the injured blood-brain barrier. *Proceedings of the National Academy of Sciences*, 113(4), 1074–1079. https://doi.org/10.1073/pnas.1520398113

Maeda, J., Higuchi, M., Inaji, M., Ji, B., Haneda, E., Okauchi, T., Zhang, M. R., Suzuki, K., & Suhara, T. (2007). Phase-dependent roles of reactive microglia and astrocytes in nervous system injury as delineated by imaging of peripheral benzodiazepine receptor. *Brain Research*, 1157, 100–111. https://doi.org/10.1016/j.brainres.2007.04.054

Nakajima, K., & Kohsaka, S. (2001). Microglia: Activation and their significance in the central nervous system. *The Journal of Biochemistry*, 130(2),169–175.

Nimmerjahn, A., Kirchhoff, F., & Helmchen, F. (2005). Resting microglial cells are highly dynamic surveillants of brain parenchyma in vivo. *Science*, 308(5726), 1314–1318. https://doi.org/1110647 [pii]10.1126/science.1110647

Owen, D. R., Gunn, R. N., Rabiner, E. A., Bennacef, I., Fujita, M., Kreisl, W. C., Innis, R. B., Pike, V. W., Reynolds, R., Matthews, P. M., & Parker, C. A. (2011). Mixed-affinity binding in humans with 18-kDa translocator protein ligands. *Journal of Nuclear Medicine*, 52(1), 24–32. https://doi.org/10.2967/jnumed.110.079459

Owen, D. R., Yeo, A. J., Gunn, R. N., Song, K., Wadsworth, G., Lewis, A., Rhodes, C., Pulford, D. J., Bennacef, I., Parker, C. A., & StJean, P. L. (2012). An 18-kDa translocator protein (TSPO) polymorphism explains differences in binding affinity of the PET radioligand PBR28. *Journal of Cerebral Blood Flow & Metabolism*, 32(1), 1–5. https://doi.org/10.1038/jcbfm.2011.147

Pannell, M., Economopoulos, V., Wilson, T. C., Kersemans, V., Isenegger, P. G., Larkin, J. R., Smart, S., Gilchrist, S., Gouverneur, V., & Sibson, N. R. (2020). Imaging of translocator protein upregulation is selective for pro-inflammatory polarized astrocytes and microglia. *Glia*, 68(2), 280–297. https://doi.org/10.1002/glia.23716

Papadopoulos, V. (1998). Structure and function of the peripheral-type benzodiazepine receptor in steroidogenic cells. *Proceedings of the Society for Experimental Biology and Medicine*, 217(2), 130–142.

Raghavendra Rao, V. L., Dogan, A., Bowen, K. K., & Dempsey, R. J. (2000). Traumatic brain injury leads to increased expression of peripheral-type benzodiazepine receptors, neuronal death, and activation of astrocytes and microglia in rat thalamus. *Experimental Neurology*, 161(1), 102–114. https://doi.org/10.1006/exnr.1999.7269 S0014-4886 (99)97269-2 [pii]

Ramlackhansingh, A. F., Brooks, D. J., Greenwood, R. J., Bose, S. K., Turkheimer, F. E., Kinnunen, K. M., Gentleman, S., Heckemann, R. A., Gunanayagam, K., Gelosa, G., & Sharp, D. J. (2011). Inflammation after trauma: Microglial activation and traumatic brain injury. *Annals of Neurology*, 70(3), 374–383. https://doi.org/10.1002/ana.22455

Rojas, S., Martín, A., Arranz, M. J., Pareto, D., Purroy, J., Verdaguer, E., Llop, J., Gomez, V., Gispert, J. D., Milián, O. Chamorro, A., & Planas, A. M. (2007). Imaging brain inflammation with [(11)C]PK11195 by PET and induction of the peripheral-type benzodiazepine receptor after transient focal ischemia in rats. *Journal of Cerebral Blood Flow & Metabolism*, 27(12), 1975–1986. https://doi.org/10.1038/sj.jcbfm.9600500

Salter, M. W., & Beggs, S. (2014). Sublime microglia: Expanding roles for the guardians of the CNS. *Cell*, *158*(1), 15–24. https://doi.org/10.1016/j.cell.2014.06.008

Sandhir, R., Onyszchuk, G., & Berman, N. E. (2008). Exacerbated glial response in the aged mouse hippocampus following controlled cortical impact injury. *Experimental Neurology*, *213*(2), 372–380 https://doi.org/10.1016/j.expneurol.2008.06.013

Savitz, S. I., & Cox, C. S., Jr. (2016). Concise review: Cell therapies for stroke and traumatic brain injury: Targeting microglia. *Stem Cells*, *34*(3), 537–542. https://doi.org/10.1002/stem.2253

Smith, H. S. (2010). Activated microglia in nociception. *Pain Physician*, *13*(3), 295–304.

Thomas, T. C., Ogle, S. B., Rumney, B. M., May, H. G., Adelson, P. D., & Lifshitz, J. (2018). Does time heal all wounds? Experimental diffuse traumatic brain injury results in persisting histopathology in the thalamus. *Behavioural Brain Research*, *340*, 137–146. https://doi.org/10.1016/j.bbr.2016.12.038

Torres-Platas, S.G., Comeau, S., Rachalski, A., Dal Bo, G., Cruceanu, C., Turecki, G., Giros, B., & Mechawar, N. (2014). Morphometric characterization of microglial phenotypes in human cerebral cortex. *Journal of Neuroinflammation*, *11*, 12. https://doi.org/10.1186/1742-2094-11-12

Wang, M., Wang, X., Zhao, L., Ma, W., Rodriguez, I. R., Fariss, R. N., & Wong, W. T. (2014). Macroglia-microglia interactions via TSPO signaling regulates microglial activation in the mouse retina. *Journal of Neuroscience*, *34*(10), 3793–3806. https://doi.org/10.1523/JNEUROSCI.3153-13.2014